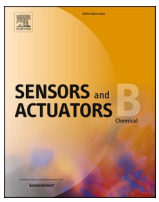
Sensors & Actuators: B. Chemical 334 (2021) 129631



Contents lists available at ScienceDirect

Sensors and Actuators: B. Chemical

journal homepage: www.elsevier.com/locate/snb





On-chip electrocatalytic NO sensing using ruthenium oxide nanorods

E. Tanumihardja [a,*], A. Paradelo Rodríguez [b], J.T. Loessberg-Zahl [a], B. Mei [b], W. Olthuis [a], A. van den Berg [a]

[a] BIOS Lab on a Chip Group, MESA+ Institute for Nanotechnology, University of Twente, Enschede, The Netherlands
[b] Photocatalytic Synthesis Group, Faculty of Science & Technology of the University of Twente, Enschede, The Netherlands

ARTICLE INFO

Keywords:
Ruthenium oxide
Electrocatalytic
Nitric oxide
Amperometric sensing
Real-time mass-spectrometry
Endothelial cells

ABSTRACT

Online, on-chip measurement of nitric oxide (NO) in organ-on-chip devices is desired to study endothelial (dys) function under dynamic conditions. In this work, ruthenium oxide (RuOx) is explored as an amperometric NO sensor and its suitability for organ-on-chip applications. For testing purposes, diethylamine NONOate was used as chemical NO donor. The NONOate's NO generation and electrochemical oxidation of generated NO were confirmed by real-time electrochemical/mass-spectrometry. Using RuOx nanorods electrodes, we show that NO oxidation occurred at a lower onset potential (+675 mV vs. Ag/AgCl) than on bare Pt electrode (+800 mV vs. Ag/AgCl). Due to NO adsorption on the RuOx surface, NO oxidation also delivered a higher current density (33.5 $nA.\mu M^{-1}.\ cm^{-2}$) compared to bare Pt (19.6 $nA.\mu M^{-1}.\ cm^{-2}$), making RuOx nanorods a favourable electrode for NO sensing applications. The RuOx electrode's suitability for organ-on-chip applications was successfully tested by using the electrode to detect a few micromolar concentration of NO generated by endothelial cell culture. Overall, the RuOx nanorods proved to be suitable for organ-on-chip studies due to their high sensitivity and selectivity. Our chip-integrated electrode allows for online NO monitoring in biologically relevant in vitro experiments.

1. Introduction

Organs-on-chips are new promising in vitro models of human tissue. The term was coined in 2010 [1], with the development of a microfluidic device able to reproduce organ-level physiology of human lungs. In this model, living human lung cells were cultured in microchannels, where mechanical forces were applied to mimic the in vivo microenvironment of the living organ. Similarly, different models have been developed to replicate a wide variety of human organs [2]. Developers of organs-on-chips hope to offer alternatives to animal models which are more ethical, physiologically representative, personalizable, and can make use of induced pluripotent stem cell technologies as well as integrated sensors [3–6].

To fully benefit from the dynamic nature of organs-on-chips, it is desirable to obtain readouts that are resolved in both space and time. Integrated microsensors can be placed within a very short distance from the cells. It would then allow real-time reading, with a time resolution down to tens of microseconds, from the living cells and/or reading from the cells' immediate microenvironment [7,8]. Micro-sized sensors have also been used to successfully get localized readouts from cell cultures, or even readings from a single cell [9,10]. These readings provide information beyond cell morphology (through microscopy) or end-point assays. Electrochemical sensors, specifically metal oxides, are often used for such devices, given their robust, miniaturizable, and reagent-free properties.

Nitric oxide (NO) is a gasotransmitter involved in a variety of human (patho)physiology. NO is most prominently released by endothelial cells, where it serves many roles in maintaining normal endothelial functions [11,12]. A large class of organ-on-chip devices involve the modelling of tissue barriers, where endothelial cells are often incorporated [2]. This makes them one of the most prevalent cell types in organ-on-chips. Furthermore, endothelial cells themselves are often at the centre of fundamental and translational *(in vitro)* studies. For example, their dysfunction (often discernible by reduced availability of NO) is closely associated with both chronic and acute cardiovascular diseases [13–15]. Online NO sensing would enable valuable studies of endothelial (dys)function in response to the dynamic and physiological conditions achieved in organs-on-chips, something which, to our knowledge, has not been reported before. Given the highly unstable nature of NO, an excellent time resolution is necessary to capture its

* Corresponding author.
E-mail address: e.tanumihardja@utwente.nl (E. Tanumihardja).

https://doi.org/10.1016/j.snb.2021.129631
Received 28 September 2020; Received in revised form 2 February 2021; Accepted 3 February 2021
Available online 9 February 2021
0925-4005/© 2021 Published by Elsevier B.V. This is an open access article under the CC BY-NC-ND license (http://creativecommons.org/licenses/by-nc-nd/4.0/).

activity in a real-time manner. This makes metal oxides electrochemical NO sensors an appropriate option for organ-on-chips applications.

NO can be electrochemically oxidized and reduced. Consequently, NO concentration can be determined electrochemically in a real-time manner. However, since the reduction potential of NO is close to that of oxygen (an inevitable component in biological studies), measurement of NO oxidation is generally preferred. NO is electrochemically oxidized in a one-electron transfer reaction. The overall irreversible reaction is given in Eq. 1 below.

$$NO + OH^- \rightarrow HNO_2 + e- \quad (1)$$

This work explores the applicability of ruthenium oxide (RuOx) as an amperometric NO sensor that is practical for use in organ-on-chip settings. Typically, NO oxidizes on metal oxides at a relatively high potential of +800 mV (vs. Ag/AgCl) [16,17] and at an even higher potential (of around +1000 mV) on carbon electrodes [18,19]. However, RuOx has been reported to have an electrocatalytic effect on NO oxidation, where NO oxidation occurs at a lower potential of +675 mV, due to the easy formation of nitrosyl complexes on the ruthenium surface [16]. This would allow us to probe the system with lower potential bias and effectively avoid interfering oxidation signal from other species (e.g. nitrite, which oxidizes at around +770 mV [20]). Therefore, RuOx would enable selective and sensitive direct NO sensing, even in a complex biological matrix [21].

In the last decade, papers on electrochemical NO sensing have reported a very broad range in sensitivity [22]. Of the reported electrodes, it is apparent that 3D (ultramicro)electrodes tend to deliver the highest sensitivity [21,23,24]. While it is well-established that the sensitivity of amperometric sensors benefits greatly from the increased mass transport, 3D (ultramicro)electrodes (e.g. modified carbon fibres) are not easy to integrate on chips. Furthermore, the use of ultramicroelectrodes would require an array design to generate sufficient current. Such an array would need a relatively large distance between the microelectrodes to be effective. This would sacrifice spatial resolution, which is a coveted advantage of on-chip sensing. In addition, the very fast response theoretically possible with ultramicroelectrode arrays is not achieved due to the sluggish oxidation reaction of NO. Therefore, we propose a robust and practical 2D electrode design for on-chip NO sensing. By modifying a flat Pt electrode with RuOx nanorods [21,25], we can study the electrocatalytic RuOx electrode for on-chip NO sensing, something that has not been reported before. Table 1 summarizes relevant works on on-chip macro electrodes tested for their NO sensitivity. Our RuOx electrodes show a current response due to NO oxidation at a lower potential than other materials while delivering high current densities. The same electrode has also been tested for its potentiometric pH and amperometric oxygen sensing performance [26], making it a simple and versatile electrode for many organ-on-chips applications.

For testing an NO sensor, it is desirable to have a source of controlled NO generation. In the late 1990s, a class of stable compounds with [N(O)NO]- functional group were synthesized for this purpose. The compound can be made to predictably breakdown and release NO [30] even at relatively low concentrations and its breakdown rate can be controlled by both pH and temperature. These compounds have since become a favourable way to generate NO, as their use is more practical and safer than bottled NO gas or chemical synthesis of NO from HNO_3 reduction. Nonetheless, NO generation as described by Keefer et al. has yet to be directly and independently confirmed by other means than electrochemical detection.

In this work, we report a novel way to confirm NO generation from diethylamine NONOate (DEANONOate) via real-time electrochemistry/mass-spectrometry (EC/MS). We also validate a novel electrocatalytic RuOx electrode for direct, real-time NO detection via the same technique. The electrode's suitability for use in organ-on-chip settings is demonstrated by its performance in an in vitro environment akin to organ-on-chip.

Table 1
Summary of on-chip macro (2D) NO sensing electrodes.

Electrode material/ design	E_{ox} (mV) vs. Ag/ AgCl	Sensitivity (nA. μM^{-1}. cm^{-2})	Electrode dimension	Ref
CA/CS/AuNP T-Macro	+795	20.2	GSA 0.495 cm^2	[27]
N-G/FePc/Nafion/ PLL ITO	+945	210	~ ⌀ 8 mm	[28]
Au nanomembrane	+800	20.6	~ 4 × 5 mm	[29]
RuOx nanorods	+675	33.5	⌀ 3 mm	This work

Abbreviations: CA, cellulose acetate; CS, chitosan; AuNP, gold nanoparticle; T-Macro, transparent macroelectrode; GSA, geometric surface area; N-G, nitrogen-doped graphene; FePc, iron(II)phthalocyanine; PLL, poly(L-lysine); ITO, indium tin oxide.

2. Experimental

2.1. DEANONOate solution preparation

Solid Diethylamine NONOate (DEANONOate from Cayman chemicals, kept at −80 °C under N_2), was used to make a stock solution of 1.5 mM DEANONOate, by dissolving 2.6 mg of the solid DEANONOate in 25 mL 10 mM NaOH that has been thoroughly deaerated. Before use, aliquots of the stock solution were also kept at −80 °C under N_2 for 2 months at most. Aliquots were also checked for their UV–vis absorbance (DEANONOate absorbance at λ = 250 nm) immediately before use. Typical absorbance spectra of DEANONOate are shown in the appendix (Fig. A14).

2.2. EC/MS experiments

Real-time electrochemistry/mass-spectrometry (EC/MS) measurements were performed using the SpectroInlets' (Copenhagen, Denmark) EC/MS system (Fig. 1) using He as the carrier gas [31]. Different m/z signals (2, 4, 32, 40, 44) were recorded over time each with 16 ms dwell time. m/z = 30 signal was recorded with 32 ms dwell time to reveal NO formation and oxidation. A three-electrodes electrochemical cell [31] was used with ⌀ 5 mm Pt disk working electrode (Pine Research), Pt wire counter electrode, and Ag/AgCl (saturated KCl) reference electrode (CH Instrument). The platinum disk electrode was polished following the routine cleaning as outlined by Pine Research. Bio-Logic VSP potentiostat was used to perform electrochemistry techniques.

EC/MS experiments were carried out using a 1.5 mM DEANONOate stock solution (in 10 mM NaOH, pH 12.076). At this point, the solution's high pH prevented the breakdown of DEANONOate. Cyclic voltammetry was performed between -0.2 and 1.1 V (vs. Ag/AgCl) at 10 mV/s scan rate (SR) to stabilize the system, before controlled DEANONOate breakdown was initiated using a controlled-current technique to drive 2 mC (200 μA for 10 s), resulting in a pH decrease triggered by the oxygen evolution reaction (OER) of water. The objective was to decrease the pH to below 10, to ensure DEANONOate breakdown. Further calculations are shown in section A3. Note that the potential was scanned down to -0.2 V to strip the platinum oxide that might have formed during the forward scan. All mass-spectrometry recordings over time were filtered with a moving average window (n = 50). Mass scans (up to m/z = 40) with 32 ms dwell time were performed before and after DEANONOate activation.

2.3. Preparation of RuOx electrode

RuOx modification was done on sputtered Pt electrodes (circular, 2.4 mm in diameter, 200 nm thick) on glass chips (Fig. 2a). The glass chips were first cleaned by sonication in isopropanol for 5 min. The substrate was then electrochemically cleaned by applying cyclic potential sweeps

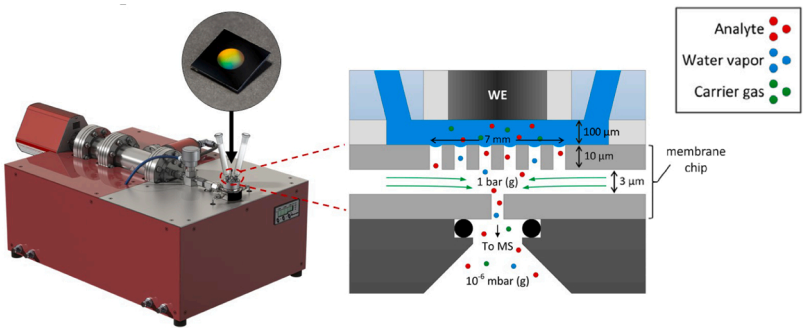


Fig. 1. EC/MS system and cross-section of its cell. Volatile molecules from the electrolyte are harvested and analysed by the MS. A Pt disk electrode was used as WE. [53,54] Adapted from original work by [31], Copyright 2018, with permission from Elsevier.

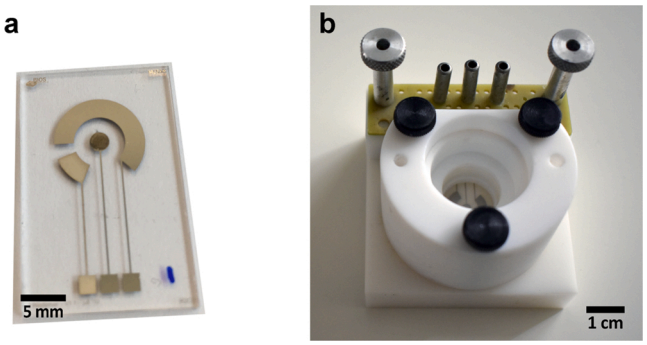


Fig. 2. (a) Glass chip with electrodes: RuOx-modified Pt WE, Ag/AgCl RE, Pt CE. (b) Teflon chip holder with pogo pins connection block.

(5 cycles with SR 200 mV/s in 0.5 M H_2SO_4 between -1 and 2 V (vs. Ag/AgCl), ending in 2 V; followed by 20 cycles with SR 100 mV/s in 0.5 M H_2SO_4 between -0.2 and 1.2 V, ending in 1.2 V). The chip was then rinsed with deionized (DI) water, blown dry with N_2, and used as RuOx substrate as previously described [25,26] with a slightly different heating protocol. In short, $Ru(OH)_3$ precursor was precipitated from 5 mM $RuCl_3$ solution, by adding 5 mM NaOH solution drop by drop. The precursor was then rinsed and resuspended in DI water. The resuspension was then dropped on the clean Pt substrate and left to dry at room temperature. The chips with $Ru(OH)_3$ precursor were baked in a pre-heated oven at 350 °C for 4 h and left in the oven to cool to room temperature (usually overnight). The resulting RuO_2 nanorods were confirmed by scanning electron microscopy (SEM) imaging.

Before every test, the electrodes (RuOx or Pt) were again electrochemically cleaned. RuOx electrodes were cycled in two steps. First, 5 cycles with SR 200 mV/s in 0.5 M H_2SO_4 between -0.2 and 1.5 V (vs. Ag/AgCl), ending in -0.2 V; followed by 20 cycles with SR 100 mV/s in 0.5 M H_2SO_4 between -0.2 and 0.7 V, ending in -0.2 V. Before measurements, the freshly cleaned RuOx electrodes were preconditioned by applying 5 potential sweeps in phosphate-buffered saline (PBS) solution (from 0.2 to 0.8 V at 10 mV/s) to build a stable oxide layer. Pt electrodes were cycled 20 times with SR 100 mV/s in 0.5 M H_2SO_4 between -0.2 and 1.2 V (vs. Ag/AgCl), ending in -0.2 V. Before the first measurement, a negative potential (-0.25 V vs. Ag/AgCl) was applied in PBS solution for 1 min to strip the oxide layer, followed by 2 potential sweeps from 0.2 to 1 V at 10 mV/s.

2.4. Electrocatalytic experiments

The RuOx electrode chip was used for most experiments unless stated otherwise. The glass chip was used with an in-house fabricated Teflon chip holder equipped with pogo pins for connection. The chip holder exposes the electrodes' active area to the electrolyte chamber (Fig. 2b). All potentials were measured against a liquid-junction Ag/AgCl (sat'd KCl) reference electrode (CH Instruments), typically placed ~5 mm from the RuOx electrode. The setup was placed inside a Faraday cage during all measurements. All measurements were carried out using Bio-Logic SP300 bipotentiostat and were performed at 22 ± 1 °C. Staircase voltammetry was carried out by scanning the potential in 10 mV step increment every 1 s, the current was sampled at the final 10% of each step.

Different amounts of the DEANONOate stock solution were diluted in PBS solution (pH 7.4) containing 27 mM KCl and 137 mM NaCl (Sigma) to make the DEANONOate concentration series. Measurements were performed after 10 min of NO formation in a closed vial. Cleaning step was always performed right before or between tests/runs to obtain comparable starting condition. All electrodes were stored in air.

2.5. Cell culture and biological experiments

Green fluorescent protein (GFP)-expressing human umbilical vein endothelial cells (HUVECs) were obtained from Cellworks. In all experiments, we started with HUVECs at passage 5. These cells were first cultured in a collagen-coated culture flask (CELLCOAT T75 flask, Greiner) using endothelial cell growth medium (EGM) from Cell Applications. The cell medium was refreshed 4 h after seeding the flask, and subsequently every 48 h. Cells reached 80% confluency after being cultured in 37 °C, 5% CO_2 incubator for 72 h and were then subcultured onto Transwell inserts as described below.

Transwell inserts (Corning Transwell, 12 mm diameter, polyester membranes with 0.4 µm pores) were covered by collagen (rat tail collagen-I from Gibco) prior to cell seeding. The apical side of the Transwell insert was covered with 0.1 mg/mL collagen in PBS solution at 7.5 µg collagen/cm^2 membrane for 45 min in the incubator. The remaining collagen solution was then aspirated and the membrane was allowed to dry under the flow hood for 30 min. Before seeding cells, collagen was rehydrated with cell medium for at least 15 min. HUVECs were obtained from an 80% confluent flask as mentioned above. The cells were released from the flask using a 0.05% trypsin-EDTA solution (Gibco) and suspended in EGM to a concentration of 1 million cells/mL before being seeded onto the collagen-covered inserts at a final density of 100.000 cells per insert. Inserts were cultured to confluency for another 24 h before measurement. Microscopy images of the cells in Transwell inserts were taken with an EVOS (EVOS M5000 Imaging System), using a GFP filter cube (AMEP4651 EVOS LED CUBE/GFP).

Right before measurement, the cultured inserts were washed two times with PBS solution and put into the autoclaved Teflon chip holder (Fig. 3) with the RuOx chip. In this configuration, the insert's membrane (with the cells on the apical side) were suspended 3 mm away from the electrodes at the basolateral side of the membrane (Fig. 3b). The basolateral side of the Transwell insert was filled with 750 µL PBS solution, and the apical side was filled with 500 µL PBS solution. Every time the insert was placed in the holder, it was inspected to make sure that no air

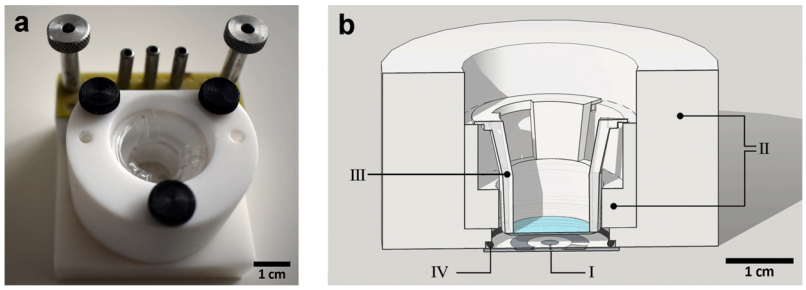


Fig. 3. Images of the setup used in the biological experiment (a) Photograph of the setup (glass chip, Teflon chip holder, pogo pins connector, and Transwell insert) (b) Cross-sectional drawing of the setup. Teflon holder (II) was made to suspend the membrane of Transwell insert (III) 3 mm above the glass chip (I), with O-ring (IV) to seal the electrochemical cell. Cells were cultured on the top (apical) side of the membrane. The spaces above (apical) and under (basolateral) the membrane were filled with PBS solution during measurements.

bubble was trapped between the electrodes and membrane. The setup with the cells was then left to equilibrate for 1 h in the incubator before measurements started.

In the biological experiments, potentials were measured against an on-board quasi Ag/AgCl reference electrode. This Ag/AgCl electrode was fabricated by anodic chloridization of sputtered Ag electrode in 1 M KCl solution for 1 h (at 13 μA/mm^2). Before the cells were introduced, the RuOx electrode was electrochemically cleaned as described in section 2.1, followed by three times rinsing with PBS solution and scanning in PBS solution. Electrochemical techniques were controlled by an EmStat 3 portable potentiostat (PalmSens).

Once the cells and setup had equilibrated in the incubator (37 °C, 5% CO_2), the chronoamperometry measurement was started by stepping the potential on the RuOx electrode up to +650 mV vs. the quasi Ag/AgCl in PBS solution (equivalent to +725 mV vs. a liquid junction Ag/AgCl RE). The slightly higher potential bias (of +725 mV vs. liquid junction Ag/AgCl instead of the previously tested +675 mV) was applied to compensate for the eventual peak shift in the more acidic environment inside the incubator. The resulting current was sampled every 0.2 s. After 400 s, different amounts of 10 mM L-arginine (Sigma) in PBS solution (filtered through 0.22 μm filter) were pipetted into the apical side of the Transwell insert, the solution was pipetted in and out several times to ensure good mixing. At 1600s after the measurement started, the Transwell insert containing the cells were taken out of the setup using tweezers. The cells viability was checked visually (using the EVOS system) after each measurement. All chronoamperometry recordings in the biological experiments were filtered with a moving average window (n = 50). Data analysis was performed in Matlab.

Additionally, a pulsed amperometry experiment was done the same way as chronoamperometry measurements, only instead of a potential step, potential pulses were applied. The potential was first held at 650 mV for 20 s, followed by 40 s of unbiased potential; this full cycle was repeated until the end of the experiment. The result plots the averaged current of the last 75% of each pulse.

3. Results and discussion

3.1. NO formation from DEANONOate

As mentioned, NONOate chemicals are preferred for in-situ NO generation. DEANONOate is a member of the NONOate class, with a half-life time of 16 min in pH 7.4 at 22 °C [30]. While the breakdown of the DEANONOate itself can be easily monitored via its absorbance at λ = 250 nm, the actual NO production has yet to be directly confirmed. So far, the NO production of DEANONOate has only been characterized electrochemically. Given the difference in the interaction between NO and different electrode materials, the signature oxidation/reduction signals of NO can be difficult to verify, especially on a novel electrode. In addition, they are often (partly) masked by other redox-active components in the solution. Here we present a new way to directly validate NO generation from DEANONOate breakdown, and validate its electrochemical signature, using a real-time EC/MS system.

Electrochemistry and mass-spectrometry measurements were started with 1.5 mM of DEANONOate in a 10 mM NaOH solution. The recorded MS data (Fig. 4a) shows the NO (m/z = 30) signal starting at a comparable baseline value to measurement in Fig. A3, confirming that the high pH prevented the DEANONOate breakdown. As shown in Fig. 4b, cyclic voltammetry (SR =10 mV/s) was performed before the DEANONOate breakdown was started. As highlighted in Fig. 4c, no redox activity from the DEANONOate was observed during cycling.

DEANONOate breakdown was initiated by lowering the pH of the solution. Since the EC/MS system had a very small working volume of 2 μL [31], it was impractical to lower the pH by liquid dosing. Therefore, we electrochemically lowered the pH via water electrolysis. After the initial potential scans, a controlled-current technique was used to supply 2 mC of charge through the system (at t = 566 s) and drive the OER (Eq. 2 below). The controlled-current technique was made sure to follow the cyclic voltammetry as it ended at +1.1 V, to guarantee that a stable oxide layer was established. Consequently, no charge would go into building an oxide layer and all of the supplied charge was assumed to directly contribute to oxygen generation via the OER. This allowed for an accurate calculation of the amount of protons produced, and consequently the change in pH. It was calculated that the 2 mC of charge delivered 20.7 nmol of protons into the 2 μL working volume, reducing the pH to 3.5. The solution was therefore considered more than acidic enough to start DEANONOate breakdown.

$$2\ H_2O \rightarrow O_2 + 4\ H^+ + 4\ e^- \quad (2)$$

As the reaction occurred, the volatile products were immediately detected by the MS. The increase in O_2 signal (M32-O2, Fig. 4a) confirmed that water oxidation occurred. The resulting pH drop was also confirmed by the potential shift of the CV features (Fig. 4c–d). Specifically, a shift in the reduction current onset of Pt oxide (with a peak around Ewe = -0.16 V vs Ag/AgCl in Fig. 4c) to a more positive potential (ΔV = +150 mV) was observed (Fig. 4d). Given the poor pH sensitivity of Pt oxide, especially in pH < 5 [32,33], a potential shift of +150 mV could indicate a decrease in pH of as much as 8.5 pH units, verifying acidification of the electrolyte.

As a consequence of the pH drop, DEANONOate breakdown and NO generation were started and volatile NO was detected (M30-NO, Fig. 4a). The signal showed a clear increase followed by a slower decay. Recorded mass-spectra (Fig. 4e) also confirmed that the NO signal (m/z = 30) increased after activation, while the measurement's baseline was unchanged. The signal at m/z = 29 also decreased visibly after the activation. Traces of several atmospheric gases (e.g. nitrogen and carbon dioxide) would show a peak at m/z = 29 when ionized by electrons. This signal might indicate a trace of dissolved atmospheric gasses present in the sample, despite the deaeration step of the sample. The signal decreased over time as the solution slowly degassed. Nonetheless, it should be noted that at such low current range, noise contribution can mislead interpretation of the mass spectrum scan. Therefore analysis in the time domain (such in Fig. 4a), which shows a clear signal change beyond an established noise level, can offer more valuable insight.

Furthermore, DEANONOate is known to break down to several by-products [30]. Traces of some of its by-products (i.e. diethylamine and N-nitrosodiethylamine) can have m/z of 30 [34,35]. However, these

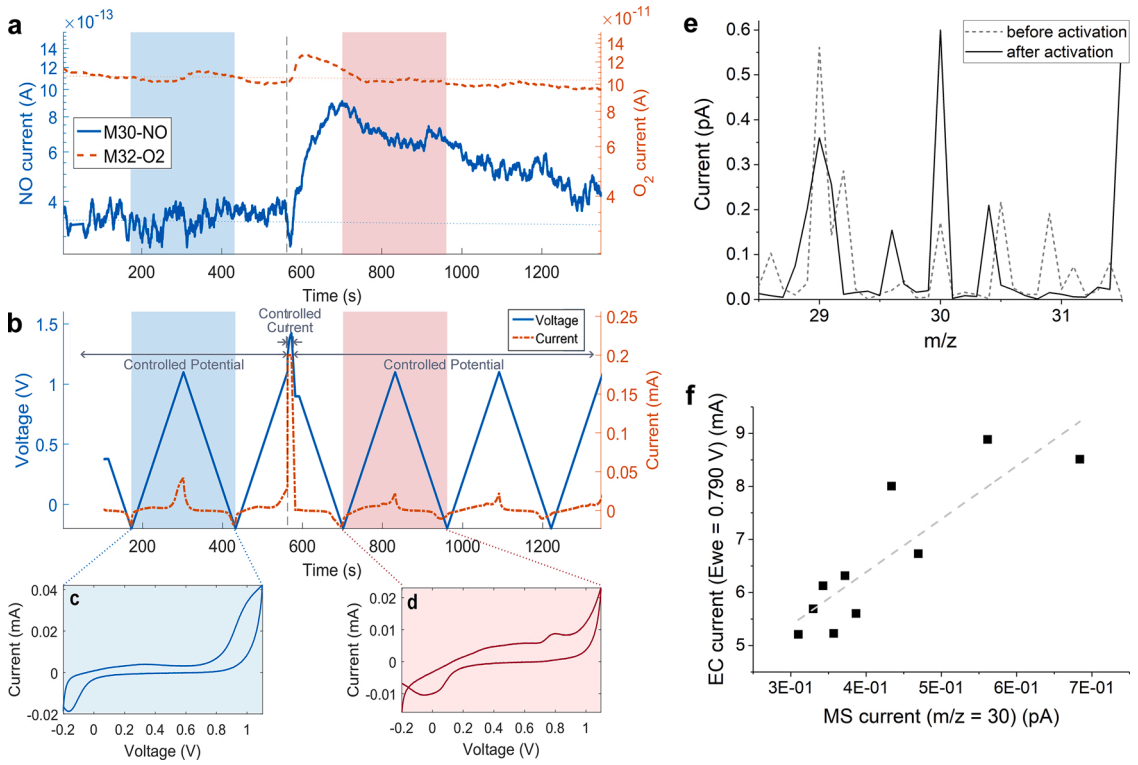


Fig. 4. (a) Recording of different m/z over time from the SpectroInlets system with 1.5 mM DEANONOate in 10 mM NaOH, the M30-NO values indicate the amount of NO ($m/z = 30$) generated over time. (b) Recording of potential (vs. Ag/AgCl) and current on the Pt WE (c) CV (SR =10 mV/s) recorded on Pt WE during voltage sweep before NO generation started (d) CV recorded after NO generation started (e) Mass scans taken before and after NO generation had started (f) Electrochemical current (measured current from each forward scan at Ewe =790 mV) plotted against MS current at the same point in time. Linear regression plot is added for visual guidance only.

by-products cannot be directly oxidized at potentials lower than +1 V under our condition [36]. Therefore, we also recorded CVs before and after activation (Fig. 4c–d). IV-curve after the activation step showed a new oxidation peak at around 790 mV (vs. sat'd Ag/AgCl), this current also correlates positively to the recorded MS current at $m/z = 30$ (Fig. 4f). Variations between the two data can be attributed mainly to the low-amplitude (therefore low signal-to-noise ratio (SNR)) MS signal. In addition, the slight peak shift of the NO oxidation signal due to the shift in pH can also introduce some variations. Given the correlation with the MS data, the peak current can be validly ascribed to NO oxidation.

3.2. RuOx nanorods fabrication results

Fig. 5 shows SEM images of the annealed RuOx electrodes. The figure shows island-like structures that are covered with rod-like RuO_2 structures with rod widths between 15−25 nm and rod lengths between 115−150 nm. The island-like structures are the amorphous $Ru(OH)_3$ precursor (the unheated precursor is shown in Fig. A1 for reference), the remaining amorphous precursor can also be seen in Fig. 5b, underneath the nanorods. Fig. 5a shows that the nanorods mostly grew on the precursor and not on the bare Pt substrate between the precursor islands. However, SEM images of the different parts of the electrode (similar to Fig. 5a) show that more than 75% of the entire electrode area was covered by RuO_2 nanorods. Longer baking time, as well as substrate preconditioning (outlined in section 2.3), resulted in improved surface coverage by smaller nanorods compared to previously reported work [26]. The resulting roughness was characterized by its capacitive current (recorded during the cleaning step, Fig. A2). The growth of nanorods typically increased the electrode's active surface area by a factor of 15−25 when compared to its geometric surface area.

3.3. Electrocatalytic NO oxidation on RuOx

Once the stable generation of NO by DEANONOate had been validated and quantified, DEANONOate was used as an NO source for

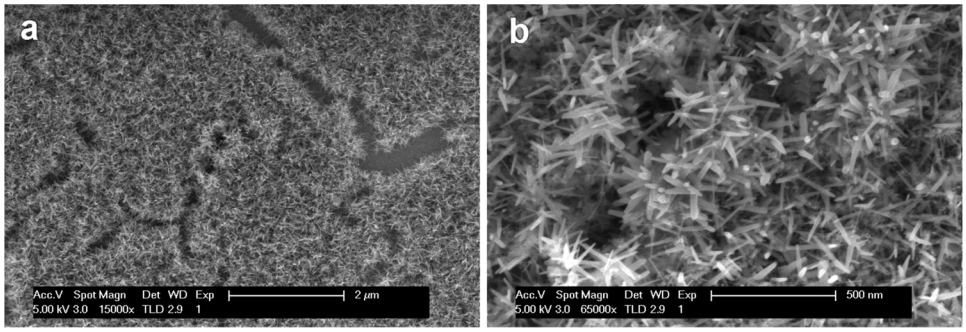


Fig. 5. SEM images of RuOx nanorods grown on Pt substrate. (a) Low magnification image showing the coverage of the RuOx nanorods, where more than 75% of the substrate area was covered by nanorods. (b) High magnification image showing the morphology of the nanorods. Most rods have a width between 15-25 nm, and a length between 115-150 nm. The nanorods grew mostly on the $Ru(OH)_3$ precursor, and the remaining precursor appears as the amorphous structures interspersed throughout the nanorods.

calibrating the response of our RuOx electrodes. Fig. 6 shows staircase voltammograms (SR =10 mV/s) recorded on RuOx and Pt electrodes in different concentrations of DEANONOate. It can be seen that NO oxidation occurred on both electrodes. The oxidation current determined for Pt in this setup closely resembled the measurements in the EC/MS system (Fig. 6b), albeit with less clear peak-shape due to the lower concentrations of NO tested. The absence of a clear peak from potential sweeps on Pt electrodes has also been reported elsewhere [37]. Nonetheless, this current was strongly correlated (R^2 = 0.99) with the DEANONOate concentration at an +800 mV vs. Ag/AgCl working electrode potential bias (Fig. 6b, inset). A similar degree of correlation was achieved at a much lower potential bias of +675 mV vs. Ag/AgCl on our RuOx electrode (Fig. 6a, inset). This is in agreement with the previously reported electrocatalytic effect of RuOx on NO oxidation.

The RuOx electrodes showed good stability, as depicted in the inset graph of Fig. 6a. The same electrode (7 months old at the time of testing), when tested 4 times within 1 week time, delivered comparable slopes and offset. On the other hand, variability between electrodes is found to be higher (Fig. A5). Four electrodes (ages between 6–11 months) were tested and compared. While they showed comparable sensitivity, they showed a larger offset range (between 3.20 and 4.69 μA), which attributed greatly to the visibly high standard deviation. Nonetheless, seeing how every electrode gave a highly linear response to NO concentrations ($R^2 > 0.99$), individually-calibrated electrodes can be used for reliable NO sensing despite the electrode to electrode variability.

It is also noteworthy that NO oxidation on Pt was found to be hindered by the presence of a Pt oxide layer. Fig. A6a shows the results of an experiment similar to that presented in Fig. 4, however, the lower limit of the potential scan was limited to +300 mV vs. Ag/AgCl. In this potential window, Pt oxide remained stable throughout the scans. As can be seen, the oxidation peak associated with NO oxidation did not appear in this experiment, regardless of the successful NO generation as confirmed by the MS measurement. Similarly, Fig. A6b compares staircase voltammograms recorded on the same Pt electrode in presence DEANONOate, where one scan took place before the stripping of the oxide layer (PtOx), and another after (Pt). The voltammogram recorded on Pt electrode shows much higher oxidation current in presence of DEANONOate than the one recorded on PtOx. This finding is in agreement with other reports, corroborating Pt oxide's reduced activity for NO oxidation when compared to Pt [38,39]. Given that Pt oxide formation is unavoidable while electrochemically driving NO oxidation, it is expected that Pt electrodes would deactivate over time when used for NO sensing.

A notable work [37] reported NO oxidation on Pt black electrode to occur at a low potential of +620 mV. However, their detection method necessitates a baseline correction due to a progressive electrode poisoning. Such baseline correction might prove unfavourable in our applications since a stable baseline might not be guaranteed in organ-on-chip studies. Furthermore, Fig. A4c–d show that the reported poisoning did not occur on our RuOx electrode under similar settings. All the abovementioned observations make RuOx the more robust electrode for (continuous) NO sensing.

Fig. A7 shows that at scan rates up to 30 mV/s, the NO oxidation current on RuOx grows linearly with the square root of the scan rate. This confirms that the system is diffusion-limited at the used SR of 10 mV/s. Therefore, while the RuOx nanorods electrodes have larger surface area compared to the bare Pt electrodes, the nanoscale roughness did not contribute to the generated current in our diffusion-limited system [40]. At the time of current sampling, the NO diffusion layer is expected to have grown to tens of micrometre thick. This distance is much larger than the scale of roughness of the RuOx electrode. As the surfaces of equal concentration tend to be averaged in the diffusion layer, the electrode appeared flat at the diffusion layer distance. Therefore, for a fair comparison, the current densities are normalized to the electrodes' geometric surface area (Fig. 6, insets). Yet, the comparison shows that the RuOx nanorods electrode delivered a higher current density than the bare Pt electrode. A similar observation has been reported [16], which can be explained by NO adsorption on the electrode surface, possibly in combination with the increased surface area and, therefore, more adsorption sites.

The nanoroughness has also been reported to be especially important for the effectiveness of NO electrodes [21,41]. The nanorough surface would be much more accessible to the small NO molecules than bigger, possibly interfering, molecules. As a preliminary experiment, the RuOx electrode was tested in a different electrode configuration using a PDMS microchannel setup (Fig. A15). Different solutions containing potentially-interfering molecules were flown in the channel to test the selectivity of the RuOx electrode. The recorded chronoamperogram (Fig. A16) showed that compared to NO, the RuOx electrode was 115 and 300 times less sensitive to $NaNO_2$ and ascorbic acid, respectively. Together with the lower oxidation potential, this makes RuOx nanorods a promising selective electrode for NO sensing in complex biological matrices, pertinent to organ-on-chip applications.

The RuOx's lower limit of detection, observed from chronoamperometry experiments (Fig. A9), was around 250 nM. The current increase in presence of ~250 nM NO was just larger than the three times standard deviation of the noise, making the signal-to-noise ratio the limiting factor. While the limit of detection is comparable to several other reports [42,43], fair comparison should include comparison of the

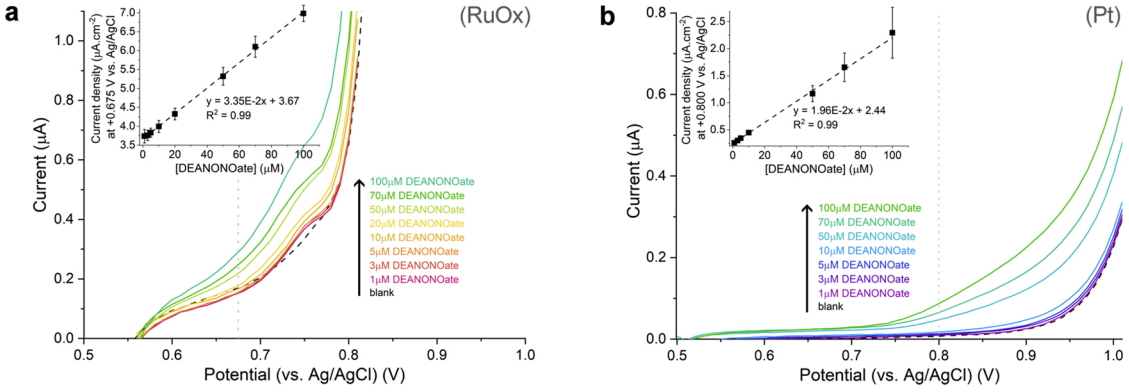


Fig. 6. (a) Staircase voltammograms (SR equivalent to 10 mV/s) recorded on a RuOx electrode in different concentrations of DEANONOate in PBS solution (pH 7.4), inset plots the calibration curve (at +675 mV, the lowest potential which is highly correlated to DEANONOate concentration) of the same electrode, error bars showing one standard deviation among the different runs (N = 4). (b) Staircase voltammograms (SR equivalent to 10 mV/s) recorded on an unmodified Pt electrode in different concentrations of DEANONOate in PBS solution (pH 7.4), inset shows calibration curve (at +800 mV, the lowest potential which is highly correlated to DEANONOate concentration) obtained from 2 electrodes each tested twice, error bars showing one standard deviation among the different runs (N = 4).

equipment's noise rating, which is difficult to achieve. Moreover, the observed limit of detection cannot be immediately translated to the expected extracellular concentrations emitted by a cells population [37]. In such setting, the detected concentration depends highly on the device design and geometry. For an accurate evaluation, experiment with cells-generated NO in a device that reflects the sensor's future application is preferred.

3.4. Signal from cells-generated NO

To show that our sensor is appropriate for measuring cell-secreted levels of NO, we demonstrate in vitro detection of the NO generated by a colony of HUVECs in response to stimulation with L-arginine. The cells used for this experiment were GFP-expressing HUVECs cells. The GFP expression was necessary for clear visualization of cells through the membrane in the Transwell inserts (Fig. 7). Endothelial cells, such as HUVECs, express an isoform of nitric oxide synthase (NOS) enzyme, which catalyzes NO synthesis from L-arginine. The catalyzed reaction is shown below [44].

$$2\ L-arginine\ +\ 3\ NADPH\ +\ 3\ H^{+} +\ 4\ O_2 \overset{\text{NOS}}{\rightarrow} 2\ citrulline\ +2\ NO\ +\ 4\ H_2O\ +\ 3\ NADP^{+} \tag{3}$$

As endothelial cells continuously synthesize NO in presence of L-arginine can be used as NO-pathway activators in in vitro experiments. Fig. 8 shows chronoamperometry measurements (at 650 mV vs. quasi Ag/AgCl or 725 mV vs. liquid junction Ag/AgCl) in 1.2 mL PBS solution in presence of HUVECs. The measurements were started in PBS solution. Different amounts of L-arginine were pipetted into the solution 400 s after the start of measurement (shown by the orange arrow in Fig. 8). As the measurement continues, 127 ± 40 s after the addition, each measurement showed a clear increase in oxidation signal. While the observed response time was higher than reported in other studies [21, 45], the system's relatively large working volume, and consequently large mass transport times, could explain such a delay. Using estimated NO diffusivity in PBS at 37 °C [46], NO molecules would take around 150 s to travel an average distance of 1 mm. The high standard deviation (40 s) among the observed response times was also directly related to how well the L-arginine was mixed into the PBS solution. Due to the constricted space of the incubator, mixing of the solution by pipetting could not be done with high consistency. This observation implies that sensor and setup miniaturization is necessary to better measure of the HUVEC's time response. Smaller distance and working volume would reduce mass transport time and, effectively, the system's response time.

The observed amperometric response was consistent with NO synthesis by cells. With all L-arginine concentrations tested, the amperometric signal displayed a rapid increase in current followed by a slow decrease. This formed a peak at 157 ± 18 s after the onset of signal increase, with peak heights that are positively correlated to the L-arginine concentration. This behaviour can be expected given the high initial concentration of L-arginine which decreased over time as it was consumed as a substrate for NO synthesis. The produced NO also slowly reacted with dissolved oxygen to form NO_2^-. Considering the interplay between the slowly diminishing NO synthesis and the NO oxidation, such peak behaviour can be expected. Fig. 8a also shows an upward current drift present at each measurement, especially noticeable after the current peaks. Control experiments (Fig. A12) also show similar upward drift that was introduced at 900 s after the start of measurements. It is conceivable that the drift is a result of extra convective flow due to thermal gradient introduced by door opening. This drift, superposed with the diminishing NO signal, could also explain the plateau-like current observed at time 900 – 1600s. As expected, the drift-ridden plateau current showed poor correlation to L-arginine concentrations, making early time current (i.e. the peak current) the better indicator of the NO production in response to the L-arginine concentration (Fig. 8b). Please note that Fig. 8b is not meant to serve as a calibration curve, rather just as an indication of correlation. Further study is necessary to determine the sensor's sensitivity to cells generated NO. Currently, our preliminary results demonstrated the RuOx electrodes' sufficient sensitivity and time resolution to monitor cell-generated NO and its dynamics in in vitro settings.

The cell colony was removed from the setup 1600s after measurement had started (indicated by black arrows in Fig. 8), effectively removing NO source from the system. The NO in the remaining PBS solution was oxidized quickly on the electrode's surface, resulting in a rapidly decreasing amperometric signal. Measured current in all experiments seemed to decrease to a lower current than their initial baseline before the signal began to increase again. This could be due to several effects. Firstly, the temperature effect might play a role, as the incubator door needed to be opened for ~1 min when removing the cells, slightly dropping the temperature of the setup. Similar current decrease was also observed after the incubator door was opened during the addition of L-arginine. Secondly, a similar response was also reported in another article [16]. While measuring at a potential higher than 675 mV (vs. Ag/AgCl (1 M KCl)), the authors also observed 'reduction-like' current after exposing electrodes to NO. The authors attributed this behaviour to attenuated oxidative background current. At such high potential, oxidation current of Cl^- or OH^- would partly make up the background current. As the electrode was exposed to NO, nitrosyl groups formed on the electrode and decreased the oxidation rate of Cl^- or OH^-. This would result in a current lower than baseline current measured before exposure to NO. As a potential bias of 725 mV (vs. Ag/AgCl (sat'd KCl)) was used in this work, the conjecture is also directly applicable to our observation.

All of the cells experiments were performed using the same chip, setup, and cell colony, they were performed sequentially in decreasing L-arginine concentrations, with a quick rinse with PBS solution in between

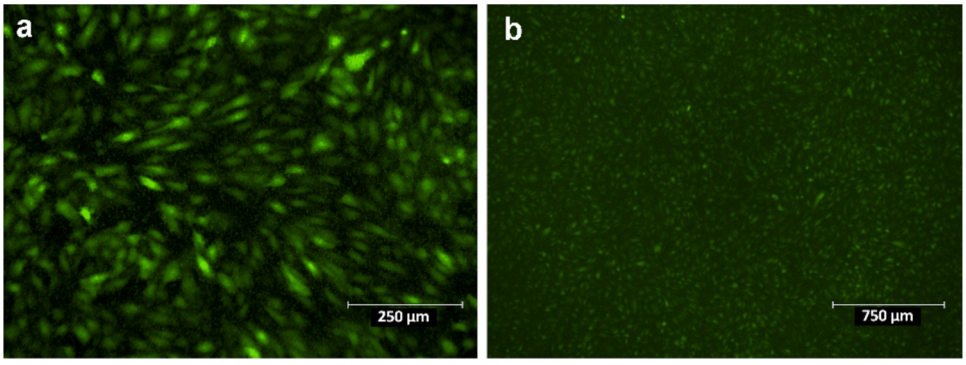


Fig. 7. Fluorescence image of HUVECs on Transwell insert cultured to confluency, taken before measurement (a) at 10x magnification (b) at 4x magnification. Speckle in images comes from imaging through the Transwell membrane.

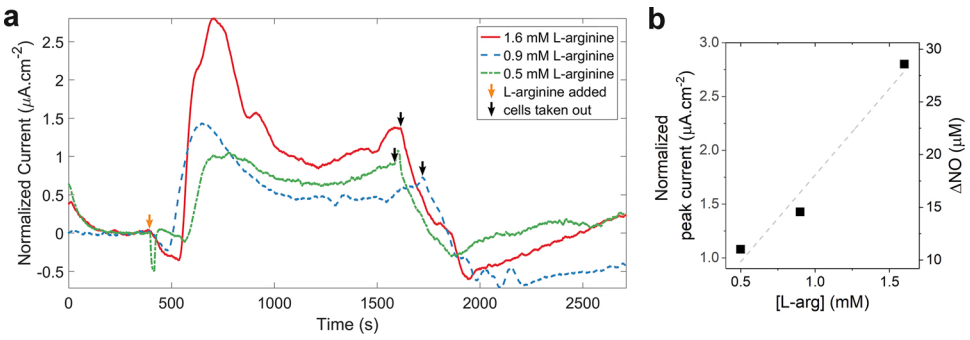


Fig. 8. (a) Normalized chronoamperometric signal in presence of HUVECs colony. Different amounts L-arginine was added at t = 400 s, noted by orange arrows. At t = 1600s, Transwell insert containing the cells was removed from the setup, noted by black arrows. The curves were normalized by subtracting each curve with its baseline current (Fig. A11). (b) Peak currents from the normalized chronoamperometry measurements are plotted against L-arginine concentration. The plot shows a good positive correlation, indicating the peaks as a response to L-arginine additions. Order-of-magnitude estimation of the corresponding change in NO concentration is given in the right axis (see section A11). Linear regression plot is added for visual guidance only.

experiments. Admittedly, the decrease of signal could be falsely correlated to L-arginine concentration, while it actually was a sign of electrode degradation. However, experiments conducted after the measurement with the lowest L-arginine concentration showed excellent signal recovery. A control experiment was conducted afterwards, using 0.9 mM L-arginine concentration (Fig. A11) and another experiment probed with a pulsed-amperometry technique (Fig. 9). The signal in both experiments recovered to the signal of the earlier experiment with the same 0.9 mM L-arginine concentration. This suggests that the electrode degradation did not (significantly) influence the monitored current in this preliminary study. Further experiments are necessary to study the sensor's degradation and lifetime. Keeping this in mind, the electrode performed reproducibly over the conducted continuous experiments (eight experiments in total, each of around one hour long) in two days' time. These experiments were representative of the expected operation of organ-on-chip sensors, where modular sensors can be prepared separately and introduced to the cell culture chip short before the continuous measurements (expected to be one to two hours long). Overall, the experiments served as a proof-of-concept of the RuOx electrodes' applicability in organ-on-chip studies. Cell colonies remained viable for at least 24 h after the measurements, indicating the PBS solution provided sufficient pH buffering capacity to maintain physiological pH during the measurement.

In addition, the true NO sensing mechanism has yet to be investigated. Under in vivo conditions, NO has been reported to form s-nitrosothiols to increase its stability [47,48], which could also take place in our biological measurement setting. For instance, s-nitrosoglutathione can be formed through many pathways involving NO, oxygen, and glutathione [49,50]; all bound to be present in our system. While this work did not differentiate the oxidation signal coming from bare NO and s-nitrosothiols, report of successful in vivo NO sensing using RuOx [21] suggests the electrode's ability to sense s-nitrosothiols. Similar to copper (typically used as catalyst in s-nitrosothiols' decomposition to release bare NO), ruthenium has high affinity to form nitrosyl complexes as well as high thiophilicity [51,52]. Therefore, it is conceivable that s-nitrosothiols decomposition is promoted on the electrode, allowing NO oxidation to occur.

The pulsed-amperometry technique was pursued to improve the amperometric signal. Especially in such a lengthy amperometry measurement, it is practically impossible to predict the current behaviour as the depletion layer grows too large and becomes unstable. Therefore, a pulsed technique is more robust for lengthy amperometry measurements. The confined, uniform pulse width results in a more defined depletion layer during each measurement. By giving the system enough time in between pulses, the concentration profile on top of the electrode is allowed to reach equilibrium with the bulk before the next pulse. Therefore, a reproducible and reliable signal can be measured over longer periods of time. The confined concentration gradient also delivered an overall higher current (Fig. 9), resulting in increased SNR. By retaining sufficient time resolution, the same dynamic captured by the conventional chronoamperometry was also clearly captured by the pulsed-amperometry technique. The aforementioned upward drift (observed at longer time scale in continuous amperometry technique) also seemed to be less apparent in the pulsed-amperometry measurement. This can suggest the drift as a ramification of the unstable continuous measurement, however, further experiments are necessary to confirm it.

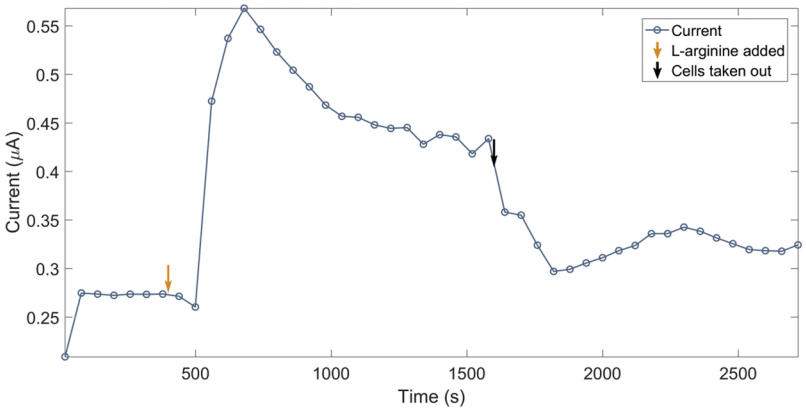


Fig. 9. Current measured by pulsed amperometry technique in presence of HUVECs. L-arginine solution was added at t = 400 s (noted by the orange arrow) to make 0.9 mM L-arginine solution. Cells were taken out at t = 1600s, noted by the black arrow. Data shown are the averaged current from the last 75% of the pulsed potential. Raw data can be found in Fig. A13.

4. Conclusions and future work

We have reported on a new method to confirm NO generation by DEANONOate, in a direct and real-time manner by means of coupled EC/MS. Via the same system, we also directly identified the electrochemical signal corresponding to NO oxidation.

We have shown RuOx nanorods to be a favourable electrocatalytic electrode for NO oxidation. NO oxidation occurred at a lower potential on RuOx electrode than on Pt. The electrocatalytic effect can be understood as the result of the concentrating effect of the RuOx surface on the NO due to ruthenium's high affinity to form nitrosyl complexes. To the same effect, NO oxidation on RuOx also delivered a higher current density than on Pt.

The lower limit of detection of NO oxidation on RuOx was tested to be around 250 nM, limited by the SNR of the current setup. Nonetheless, we demonstrated the RuOx based sensor to have high enough sensitivity for organ-on-chip applications and biological experiments. Amperometric measurement on RuOx electrodes successfully monitored NO down to the low micromolar concentration as generated by a colony of endothelial cells. We also demonstrated a pulsed-amperometry technique as an improvement over conventional chronoamperometry for lengthy amperometric measurements. The preliminary cell biology results serve as a proof-of-concept, which suggest that RuOx is a versatile electrode material for organ-on-chip technologies. Future work will include miniaturization and on-chip integration of the RuOx electrode and its application in biologically-relevant studies.

CRediT authorship contribution statement

E. Tanumihardja: Conceptualization, Methodology, Investigation, Writing - original draft, Visualization. **A. Paradelo Rodríguez:** Conceptualization, Methodology, Investigation, Writing - review & editing. **J.T. Loessberg-Zahl:** Conceptualization, Methodology, Investigation, Writing - review & editing. **B. Mei:** Conceptualization, Methodology, Writing - review & editing, Supervision. **W. Olthuis:** Conceptualization, Methodology, Writing - review & editing, Supervision, Funding acquisition. **A. van den Berg:** Writing - review & editing, Supervision, Funding acquisition.

Declaration of Competing Interest

The authors declare that they have no known competing financial interests or personal relationships that could have appeared to influence the work reported in this paper.

Acknowledgements

This research was funded by the European Research Council (ERC) under the European Union's Horizon 2020 research and innovation programme (grant agreement n^{o} 669768, VESCEL project).

Great thanks are extended to Andries van der Meer and Mathieu Odijk for their valuable scientific input. Many thanks are also extended to Paul ter Braak and Elsbeth Bossink for their input and help especially for the biological experiments. Authors are also deeply grateful of Johan Bomer for his technical input and assistance, of Hans de Boer for his work in the fabrication of chip-holder, and of Jasper Lozeman for the discussions about mass-spectrometry and his input in manuscript preparation.

Appendix A. Supplementary data

Supplementary material related to this article can be found, in the online version, at doi:https://doi.org/10.1016/j.snb.2021.129631.

References

[1] D. Huh, B.D. Matthews, A. Mammoto, M. Montoya-Zavala, H.Y. Hsin, D.E. Ingber, Reconstituting organ-level lung functions on a chip, Science (80-.) 328 (2010) 1662–1668, https://doi.org/10.1126/science.1188302.

[2] B. Zhang, A. Korolj, B.F.L. Lai, M. Radisic, Advances in organ-on-a-chip engineering, Nat. Rev. Mater. 3 (2018) 257–278, https://doi.org/10.1038/s41578-018-0034-7.

[3] S.N. Bhatia, D.E. Ingber, Microfluidic organs-on-chips, Nat. Biotechnol. 32 (2014) 760–772, https://doi.org/10.1038/nbt.2989.

[4] A. Cochrane, H.J. Albers, R. Passier, C.L. Mummery, A. van den Berg, V.V. Orlova, A.D. van der Meer, Advanced in vitro models of vascular biology: human induced pluripotent stem cells and organ-on-chip technology, Adv. Drug Deliv. Rev. 140 (2019) 68–77, https://doi.org/10.1016/j.addr.2018.06.007.

[5] A. Van Den Berg, C.L. Mummery, R. Passier, A.D. Van der Meer, Personalised organs-on-chips: functional testing for precision medicine, Lab Chip 19 (2019) 198–205, https://doi.org/10.1039/c8lc00827b.

[6] M.W. van der Helm, O.Y.F. Henry, A. Bein, T. Hamkins-Indik, M.J. Cronce, W. D. Leineweber, M. Odijk, A.D. van der Meer, L.I. Segerink, D.E. Ingber, Non-invasive sensing of transepithelial barrier function and tissue differentiation in organs-on-chips using impedance spectroscopy, Lab Chip 19 (2019) 452–463, https://doi.org/10.1039/c8lc00129d.

[7] J. Kieninger, A. Weltin, H. Flamm, G.A. Urban, Microsensor systems for cell metabolism-from 2D culture to organ-on-chip, Lab Chip 18 (2018) 1274–1291, https://doi.org/10.1039/c7lc00942a.

[8] Kratz, Höll, Schuller, Ertl, Rothbauer, Latest trends in Biosensing for microphysiological Organs-on-a-Chip and Body-on-a-Chip systems, Biosensors 9 (2019) 110, https://doi.org/10.3390/bios9030110.

[9] Y. Li, A. Meunier, R. Fulcrand, C. Sella, C. Amatore, L. Thouin, F. Lemaître, M. Guille-Collignon, Multi-chambers microsystem for simultaneous and direct electrochemical detection of reactive oxygen and nitrogen species released by cell populations, Electroanalysis 28 (2016) 1865–1872, https://doi.org/10.1002/elan.201501157.

[10] T. Malinski, Z. Taha, Nitric oxide release from a single cell measured in situ by a porphyrinic-based microsensor, Nature 358 (1992) 676–678, https://doi.org/10.1038/358676a0.

[11] R.O. Cannon, Role of nitric oxide in cardiovascular disease: focus on the endothelium, Clin. Chem. 44 (1998) 1809–1819.

[12] D. Tousoulis, A.-M. Kampoli, C. Tentolouris Nikolaos Papageorgiou, C. Stefanadis, The role of nitric oxide on endothelial function, Curr. Vasc. Pharmacol. 10 (2012) 4–18, https://doi.org/10.2174/157016112798829760.

[13] M.I. Bogorad, J. DeStefano, J. Karlsson, A.D. Wong, S. Gerecht, P.C. Searson, Review: in vitro microvessel models, Lab Chip 15 (2015) 4242–4255, https://doi.org/10.1039/C5LC00832H.

[14] Jyi Chen, Zxin Ye, Xfen Wang, J. Chang, Mwen Yang, Hhua Zhong, Ffang Hong, Slong Yang, Nitric oxide bioavailability dysfunction involves in atherosclerosis, Biomed. Pharmacother. 97 (2018) 423–428, https://doi.org/10.1016/j.biopha.2017.10.122.

[15] H.A.R. Hadi, C.S. Carr, J. Al Suwaidi, Endothelial dysfunction: cardiovascular risk factors, therapy, and outcome, Vasc. Health Risk Manag. 1 (2005) 183–198.

[16] B.W. Allen, C.A. Piantadosi, L.A. Coury, Electrode materials for nitric oxide detection, Nitric Oxide 4 (2000) 75–84, https://doi.org/10.1006/niox.2000.0273.

[17] K. Shibuki, An electrochemical microprobe for detecting nitric oxide release in brain tissue, Neurosci. Res. 9 (1990) 69–76, https://doi.org/10.1016/0168-0102(90)90048-J.

[18] S.A. Bhat, S.A. Pandit, M.A. Rather, G.M. Rather, N. Rashid, P.P. Ingole, M.A. Bhat, Self-assembled AuNPs on sulphur-doped graphene: a dual and highly efficient electrochemical sensor for nitrite (NO2-) and nitric oxide (NO), New J. Chem. 41 (2017) 8347–8358, https://doi.org/10.1039/c7nj01565h.

[19] M.D. Brown, M.H. Schoenfisch, Catalytic selectivity of metallophthalocyanines for electrochemical nitric oxide sensing, Electrochim. Acta 273 (2018) 98–104, https://doi.org/10.1016/j.electacta.2018.03.139.

[20] T. Dodevska, I. Shterev, Y. Lazarova, An electrochemical sensing platform based on iridium oxide for highly sensitive and selective detection of nitrite and ascorbic acid, Acta Chim. Slov. 65 (2018) 970–979, https://doi.org/10.17344/acsi.2018.4672.

[21] S.J. Kim, H. Jung, C. Lee, M.H. Kim, Y. Lee, Biological application of RuO2 nanorods grown on a single carbon fiber for the real-time direct nitric oxide sensing, Sensors Actuators B Chem. 191 (2014) 298–304, https://doi.org/10.1016/j.snb.2013.09.103.

[22] M.D. Brown, M.H. Schoenfisch, Electrochemical nitric oxide sensors: principles of design and characterization, Chem. Rev. 119 (2019) 11551–11575, https://doi.org/10.1021/acs.chemrev.8b00797.

[23] Z. Liu, A. Nemec-Bakk, N. Khaper, A. Chen, Sensitive electrochemical detection of nitric oxide release from cardiac and Cancer cells via a hierarchical nanoporous gold microelectrode, Anal. Chem. 89 (2017) 8036–8043, https://doi.org/10.1021/acs.analchem.7b01430.

[24] S.R. Ng, C.X. Guo, C.M. Li, Highly sensitive nitric oxide sensing using three-dimensional Graphene/Ionic liquid nanocomposite, Electroanalysis 23 (2011) 442–448, https://doi.org/10.1002/elan.201000344.

[25] Z.G. Chen, F. Pei, Y.T. Pei, J.T.M. De Hosson, A versatile route for the synthesis of single crystalline oxide nanorods: growth behavior and field emission characteristics, Cryst. Growth Des. 10 (2010) 2585–2590, https://doi.org/10.1021/cg901558n.

[26] E. Tanumihardja, W. Olthuis, A. van den Berg, Ruthenium oxide nanorods as potentiometric pH sensor for organs-on-chip purposes, Sensors 18 (2018) 2901, https://doi.org/10.3390/s18092901.
[27] J. Elliott, J. Duay, O. Simoska, J.B. Shear, K.J. Stevenson, Gold nanoparticle modified transparent carbon ultramicroelectrode arrays for the selective and sensitive electroanalytical detection of nitric oxide, Anal. Chem. 89 (2017) 1267–1274, https://doi.org/10.1021/acs.analchem.6b03987.
[28] H. Xu, C. Liao, Y. Liu, B.C. Ye, B. Liu, Iron phthalocyanine decorated nitrogen-doped graphene biosensing platform for real-time detection of nitric oxide released from living cells, Anal. Chem. 90 (2018) 4438–4444, https://doi.org/10.1021/acs.analchem.7b04419.
[29] R. Li, H. Qi, Y. Ma, Y. Deng, S. Liu, Y. Jie, J. Jing, J. He, X. Zhang, L. Wheatley, C. Huang, X. Sheng, M. Zhang, L. Yin, A flexible and physically transient electrochemical sensor for real-time wireless nitric oxide monitoring, Nat. Commun. 11 (2020), https://doi.org/10.1038/s41467-020-17008-8.
[30] L.K. Keefer, R.W. Nims, K.M. Davies, D.A. Wink, "NONOates" (1-substituted diazen-1-ium-1,2-diolates) as nitric oxide donors: convenient nitric oxide dosage forms, Meth. Enzymol. (1996) 281–293, https://doi.org/10.1016/S0076-6879(96)68030-6.
[31] D.B. Trimarco, S.B. Scott, A.H. Thilsted, J.Y. Pan, T. Pedersen, O. Hansen, I. Chorkendorff, P.C.K.K. Vesborg, Enabling real-time detection of electrochemical desorption phenomena with sub-monolayer sensitivity, Electrochim. Acta 268 (2018) 1–13, https://doi.org/10.1016/j.electacta.2018.02.060.
[32] A. Fog, R.P. Buck, Electronic semiconducting oxides as pH sensors, Sens. Actuators 5 (1984) 137–146, https://doi.org/10.1016/0250-6874(84)80004-9.
[33] K.G. Kreider, M.J. Tarlov, J.P. Cline, Sputtered thin-film pH electrodes of platinum, palladium, ruthenium, and iridium oxides, Sensors Actuators B. Chem. 28 (1995) 167–172, https://doi.org/10.1016/0925-4005(95)01655-4.
[34] SDBSWeb, MS-NW-0717 SDBS NO. 513 [WWW Document], Natl. Inst. Adv. Ind. Sci. Technol., 1999. URL https://sdbs.db.aist.go.jp (accessed 5.19.20).
[35] SDBSWeb, MS-NW-2884 SDBS NO. 5340 [WWW Document], Natl. Inst. Adv. Ind. Sci. Technol., 1999. URL https://sdbs.db.aist.go.jp (accessed 5.19.20).
[36] M. Jonsson, D.D.M. Wayner, J. Lusztyk, Redox and acidity properties of alkyl- and arylamine radical cations and the corresponding aminyl radicals, J. Phys. Chem. 100 (1996) 17539–17543, https://doi.org/10.1021/jp961286q.
[37] Y. Li, C. Sella, F. Lemaître, M. Guille-Collignon, L. Thouin, C. Amatore, Electrochemical Detection of Nitric Oxide and Peroxynitrite Anion in Microchannels at Highly Sensitive Platinum-Black Coated Electrodes. Application to ROS and RNS Mixtures prior to Biological Investigations, Electrochim. Acta 144 (2014) 111–118, https://doi.org/10.1016/j.electacta.2014.08.046.
[38] A.C.A. de Vooys, G.L. Beltramo, B. van Riet, J.A.R. van Veen, M.T.M. Koper, Mechanisms of electrochemical reduction and oxidation of nitric oxide, Electrochim. Acta 49 (2004) 1307–1314, https://doi.org/10.1016/j.electacta.2003.07.020.
[39] W. Hauptmann, M. Votsmeier, J. Gieshoff, A. Drochner, H. Vogel, Inverse hysteresis during the NO oxidation on Pt under lean conditions, Appl. Catal. B Environ. 93 (2009) 22–29, https://doi.org/10.1016/j.apcatb.2009.09.008.
[40] A.J. Bard, L.R. Faulkner, Electrochemical Methods: Fundamentals and Applications, John Wiley & Sons, Inc., 2001.
[41] B.W. Allen, C.A. Piantadosi, Electrochemical activation of electrodes for amperometric detection of nitric oxide, Nitric Oxide - Biol. Chem. 8 (2003) 243–252, https://doi.org/10.1016/S1089-8603(03)00029-6.
[42] X. Dang, H. Hu, S. Wang, S. Hu, Nanomaterials-based electrochemical sensors for nitric oxide, Microchim. Acta 182 (2014) 455–467, https://doi.org/10.1007/s00604-014-1325-3.
[43] M. Govindhan, Z. Liu, A. Chen, Design and electrochemical study of platinum-based nanomaterials for sensitive detection of nitric oxide in biomedical applications, Nanomaterials 6 (2016), https://doi.org/10.3390/nano6110211.
[44] R.G. Knowles, S. Moncada, Nitric oxide synthases in mammals, Biochem. J. 298 (1994) 249–258, https://doi.org/10.1042/bj2980249.
[45] S. Jiang, R. Cheng, X. Wang, T. Xue, Y. Liu, A. Nel, Y. Huang, X. Duan, Real-time electrical detection of nitric oxide in biological systems with sub-nanomolar sensitivity, Nat. Commun. 4 (2013) 1–16, https://doi.org/10.1038/ncomms3225.
[46] I.G. Zacharia, W.M. Deen, Diffusivity and solubility of nitric oxide in water and saline, Ann. Biomed. Eng. 33 (2005) 214–222, https://doi.org/10.1007/s10439-005-8980-9.
[47] B.W. Allen, J.S. Stamler, C.A. Piantadosi, Hemoglobin, nitric oxide and molecular mechanisms of hypoxic vasodilation, Trends Mol. Med. 15 (2009) 452–460, https://doi.org/10.1016/j.molmed.2009.08.002.
[48] Z. Liu, M.A. Rudd, J.E. Freedman, J. Loscalzo, S-Transnitrosation reactions are involved in the metabolic fate and biological actions of nitric oxide, J. Pharmacol. Exp. Ther. 284 (1998) 526–534.
[49] A. Keszler, Y. Zhang, N. Hogg, Reaction between nitric oxide, glutathione, and oxygen in the presence and absence of protein: how are S-nitrosothiols formed? Free Radic. Biol. Med. 48 (2010) 55–64, https://doi.org/10.1016/j.freeradbiomed.2009.10.026.
[50] J.S. Stamler, D.I. Simon, J.A. Osborne, M.E. Mullins, O. Jaraki, T. Michel, D. J. Singel, J. Loscalzo, S-Nitrosylation of proteins with nitric oxide: synthesis and characterization of biologically active compounds, Proc. Natl. Acad. Sci. U. S. A. 89 (1992) 444–448, https://doi.org/10.1073/pnas.89.1.444.
[51] A. Lutzke, A.C. Melvin, M.J. Neufeld, C.L. Allison, M.M. Reynolds, Nitric oxide generation from S-nitrosoglutathione: New activity of indium and a survey of metal ion effects, Nitric Oxide - Biol. Chem. 84 (2019) 16–21, https://doi.org/10.1016/j.niox.2019.01.005.
[52] G.B. Richter-Addo, Binding of organic nitroso compounds to metalloporphyrins, Acc. Chem. Res. 32 (1999) 529–536, https://doi.org/10.1021/ar970351r.
[53] SpectroInlets, Working Principle of the Membrane Chip [WWW Document], URL, 2019, https://spectroinlets.com/working-principle-of-the-membrane-chip/.
[54] D.B. Trimarco, T. Pedersen, O. Hansen, I. Chorkendorff, P.C.K. Vesborg, Fast and sensitive method for detecting volatile species in liquids, Rev. Sci. Instrum. 86 (2015), 075006, https://doi.org/10.1063/1.4923453.

Esther Tanumihardja received her Master in Sensor System Engineering at Hanze University of Applied Sciences in 2016. She is a PhD student at University of Twente's BIOS Lab on a Chip group. Her research interests include novel applications of electrochemical sensing and techniques.

Ainoa Paradelo Rodríguez obtained her Master in Chemical Engineering at Universidad Autónoma de Madrid and Universidad Rey Juan Carlos. She is a Ph.D. student of University of Twente at the PhotoCatalytic Synthesis group. Her research focused on the fundamental understanding of electrochemical reactions.

Joshua Loessberg-Zahl received a PhD from the University of Twente in 2019. He is currently a post-doctoral researcher there at the BIOS Lab on a Chip group. His research interests include micro and nano fluidics as well as the development of techniques to control the chemical microenvironment of cell cultures.

Bastian Mei (Photocatalytic Synthesis Group and MESA + Institute for Nanotechnology, University of Twente) studied chemistry with major in industrial chemistry at the Ruhr-University Bochum (Germany). After two years as a Postdoctoral researcher at the Technical University of Denmark (group of Ib Chorkendorff) he joined the University of Twente, where he is currently an Assistant Professor. His research is focused on the development of light- and electricity-driven processes with a particular emphasis on sustainable hydrogen production, selective oxidation of water and selective oxidation of organic molecules to valuable products.

Wouter Olthuis received his MSc. degree in electrical engineering from the University of Twente, Enschede, the Netherlands and then joined the Center for MicroElectronics, Enschede (CME) doing research on inorganic electric materials for subminiature silicon microphones. He received the PhD degree from the Biomedical Engineering Division of the Faculty of Electrical Engineering, University of Twente, in 1990. The subject of his dissertation was the use of iridium oxide in ISFET-based coulometric sensor-actuator devices. Since 1991 he has been working as an Assistant Professor in the Laboratory of Biosensors, part of the MESA + Research Institute of the University of Twente. Currently, he is Associate Professor in the BIOS Lab-on-Chip group of the MESA + Institute of Nanotechnology and is responsible for the theme Electrochemical sensors and Sensor systems. He has (co-)authored over 190 papers (h = 40) and 7 patents. From 2006 until 2011 he has also been the Director of the Educational Programme of Electrical Engineering at the Faculty of Electrical Engineering, Mathematics and Computer Science at the University of Twente. In 2011, he was appointed as officer on education in the executive committee of the IEEE Benelux section.

Prof. Albert van den Berg is a full professor of University of Twente, a member of Royal Dutch Academy of Science. He received his BS, MS and PhD from University of Twente in 1981, 1983 and 1988, respectively, with the background of Applied Physics and Applied Science and Technology. He is a pioneer and active member in nanotechnology, microfluidics and lab-on-a-chip research areas. His research interests include fundamentals and applications of microfluidics in sensors, actuators, biology and electronic devices.